ACCELERATION AND DRIFT REDUCTION OF MOX GAS SENSORS USING ACTIVE SIGMA-DELTA CONTROLS BASED ON DIELECTRIC EXCITATION

N. Solà-Peñafiel[1,2], X. Manyosa[1], E. Navarrete[2], J. Ramos-Castro[1], V. Jiménez[1], S. Bermejo[1], I. Gracia[3], E. Llobet[2], M. Domínguez-Pumar[1*]

[1]Micro and Nano Technologies Group, Electronic Eng. Dept., Universitat Politècnica de Catalunya, Barcelona, Spain.
[2]MINOS-EMaS, Department d'Enginyeria Electronica, Universitat Rovira i Virgili, Tarragona, Spain.
[3]Instituto de Microelectrónica de Barcelona (IMB-CNM, CSIC), Campus UAB, 08193, Bellaterra, Spain
*email: manuel.dominguez@upc.edu

ABSTRACT

The objective of this paper is to apply a closed-loop control based on dielectric excitation to MOX gas sensors in order to improve their response time. The control implements a feedback loop in which temperature modulations keep constant the sensor reactance, measured at constant temperature. The required fast temperature switching has been implemented on MEMS microhotplates. The mean temperature generated by the control is the new output signal. This technique is applied to an in-house sensor made of WO_3 nanowires decorated with gold nanoparticles to detect NH_3 and to a commercial MEMS MOX sensor (CCS801).

KEYWORDS

Gas sensor, control, metal oxide, dielectric excitation.

1 INTRODUCTION

In today's world, VOC's air concentration detectors [1], exhaust gas sensors in the automotive industry [2,3], ammonia sensors in livestock farms to control animal welfare [4], or selective gas sensors for gas leaks in chemical industries [5] are some of the applications where gas sensors have a market. For this reason, interest in metal-oxide gas sensors (MOX) has been increased in recent years [6,7]. Despite the advantages, these sensors may present a lack of selectivity, large response times and long-term drifts [8]. Dynamic models have been proposed to describe the transient response using nonlinear methods [9,10]. Some of these works use neural networks [11,12], PCA separation [13,14], reservoir computing [15], support vector machines [16] or instabilities corrections [17].

Additionally, temperature-cycled operation has been used with MOX gas sensors in order to classify chemical compounds [18,19]. By generating periodical temperature patterns and analysing the transient responses in the conductivity of the sensor, the selectivity of the sensor can be improved, such as in the case of the Differential Surface Reduction (DSR), [18]. Typically, the duration of the temperature cycles goes from some seconds to minutes. The time response is improved in some cases, since the open loop temperature cycling has been observed to accelerate transient changes in the conductance of the sensor [20].

Alternatively, it has been proposed to operate sensors under constant surface potential [21-23]. An active discrete-time control circuit, implementing fast temperature switching, keeps constant the resistivity of the sensing layer, measured at a reference temperature, at which the system comes back recurrently, during each sampling period. The temperature of the sensing layer is neither constant, nor periodical. The control adjusts the average temperature of the temperature waveforms in order to achieve constant surface potential operation (sliding mode control). By operating the sensor in this way, typically response times are significantly reduced. The same type of operation has been shown to accelerate the time response in thermal sensors [24].

The objective of this paper now is to explore the possibility of implementing a control feedback loop using the sensor reactance as the main feedback signal, instead of the resistivity of the sensor. It has very recently demonstrated in [25] that the open-loop reactance response of MOX sensors is more linear and recovery times can be reduced. Now, in this paper we will show that sensor reactance can also be used as feedback signal when operating the sensors under constant surface potential. And that reactance-based closed-loop operation can also be used to improve the open-loop reactance response of the sensor. Experimental measurements will be presented using a commercial sensor (CCS801) and another fabricated in-house, made of Au-loaded WO_3 nanowires.

2 CLOSED-LOOP CONTROL

The system that has been implemented includes two nested controls. The first one is based on a Wheatstone bridge with feedback to control the instantaneous temperature of the microhotplate (see **Fig. 1**). It is a very well-known

circuit that has been used for implementing constant temperature operation in high-bandwidth hotwire anemometers [26,27]. The circuit is configured to enforce two different temperatures, either T_{High} or T_{Low}. The value of these temperatures can be optimized for each sensor and expected environment. The output voltage of the operational amplifier dissipates a power on R_{heater} increasing its temperature until its resistance is equal to the pairing resistor in the other branch (R_{low} or R_{high}). The digital signal *Sel* controls the analog multiplexer in order to select any of the two working temperatures. Since it is an active circuit using feedback in the thermal domain, the response time of the temperature transitions can be shorter than the value of open-loop thermal constants (typically in the range 5-10 ms for the microhotplates used in this work). Snapshot examples are shown later in this section.

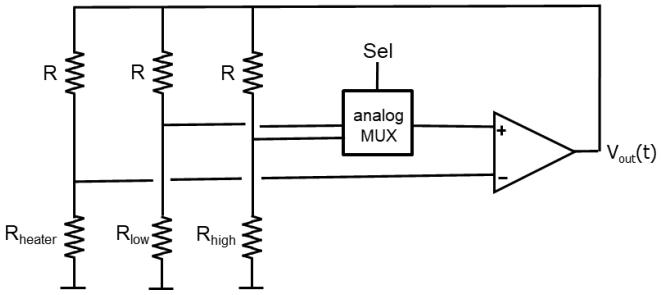

Fig. 1. Schematic concept of the temperature control circuit. The *Sel* signal at the input of the analog multiplexor is used to set one of the two temperatures in the control, and is driven by the digital circuitry to ensure the necessary fast switching temperature waveforms.

The second nested control is shown in **Fig.2**. The goal of this control is to keep constant the reactance of the sensing layer, measured at constant temperature, applying fast temperature switching. This control is achieved by generating an adequate average temperature in the sensing layer. The novel approach of this paper is that the control is applied now to the reactance at a certain frequency of the sensing layer impedance, instead of the real part of the impedance as in previous works [21-23,28].

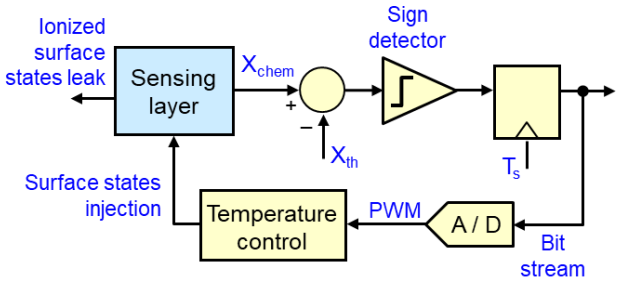

Fig. 2. First-order sigma-delta control implementing dielectric excitation. The objective of the control is to enforce a constant value, X_{th}, of the reactance of the sensing layer, X_{chem}.

The actuation uses a Pulse Width Modulator (PWM) as integrator, providing more quantization steps per sampling period than a 1-bit sigma-delta. The variable temperature profiles have two different parts. During the first 100 ms the changes in the average temperature take place. In this time interval, the temperature can be T_{High} or T_{Low}, depending on the instantaneous value of the PWM signal generated by the control. The second part, with a duration of 150 ms, is when the impedance analyser takes the measurements. The temperature profiles for the extreme values of the PWM signal (0 and 100) can be seen in **Fig.3**.

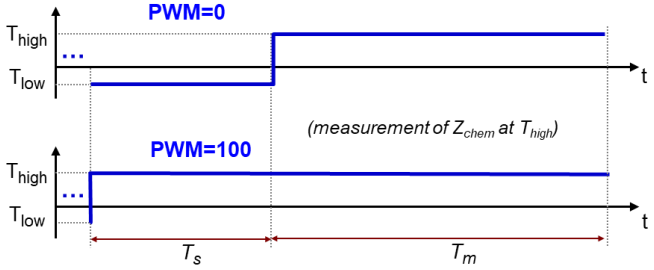

Fig. 3. Temperature waveforms generated by the control for the extreme values of the PWM signal (0 and 100). During the first time interval, T_s=100 ms, temperature changes as a function of the PWM value. During the second interval, T_m=150 ms, temperature is kept constant (T_{high}) and the impedance of the sensing layer is measured.

T_{High} and T_{Low} must be chosen in view of the sensing layer sensitivity and the thermal dynamics of the microhotplate, [28]. Typically, T_{High} must be high enough so that the sensor is sensitive to the gas to be detected, while T_{Low} must be low in order to appreciably change the average temperature for low PWM values. In any case, the thermal dynamics of the complete system must be considered because a very large temperature difference may require longer stabilization times.

Fig.4 shows examples of the transient temperature waveforms obtained with the temperature control circuit, and one of the sensors used in the experiments (CCS801), for two PWM values: 20 and 100. As it can be observed, temperature switching between T_{high} and T_{low} is very fast (< 5 ms). In this case T_{high} = 340°C and T_{low} =240°C. The power peaks at the transitions, generated by the large bandwidth temperature control, ensure temperature transitions smaller than the time constants associated with the sensor MEMS membrane (~10 ms).

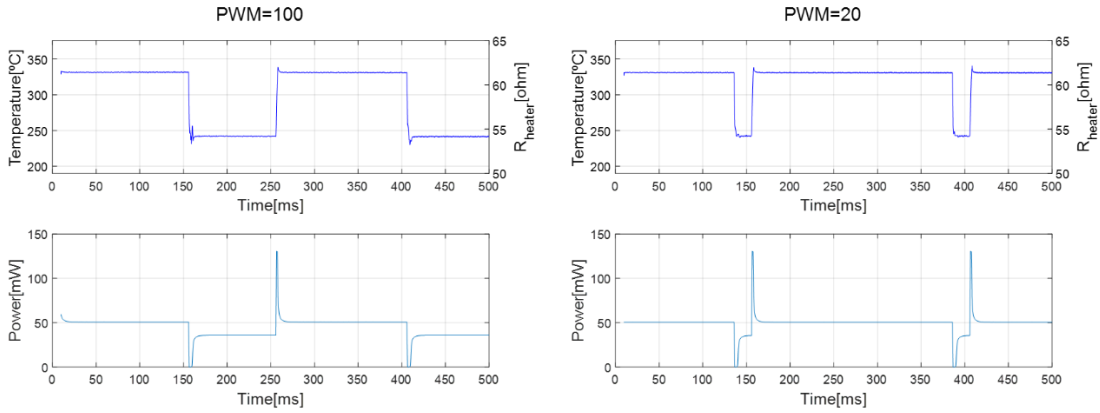

Fig. 4. Examples of temperature switching waveforms obtained with the circuit in Fig. 1. (Left) Instantaneous temperature and applied power in the case of having a PWM value of 100. (Right) Idem for a PWM value of 20. The power peaks at the transitions are generated by the circuit in order to guarantee fast switching times (< 5ms). Reactance is measured during the last 150 ms of the waveform (at high temperature).

The objective of the controls implemented in previous works [21-23,28]., is to accelerate the time response of the sensor by operating the sensor under constant surface potential. In the case of n-type semiconductors, the conductance of the sensor, G, is typically modelled as [18,21]:

$$G = G_0(T)e^{-\frac{qV_s}{k_BT}}$$

Where $G_0(T)$is a prefactor, $k_B$is the Boltzmann constant, T is the temperature, q is the electron charge and $V_s$is the potential associated to the energy barrier of the depletion zone near the surface of the semiconductor due to ionosorption of chemical species. This conductance model is an example of a system presenting fast-slow dynamics. Rapid temperature switching generates fast redistribution of carriers in the semiconductor, while the time evolution of the surface potential has much slower dynamics, since it is linked to changes in the ionosorbed species concentrations, and therefore responds to the average value of the temperature.

The control implements fast temperature switching with two objectives:

- 1st objective: monitor changes in V_s, by fast switching to a reference temperature, T_{high}, at each sampling period (T_s). The feedback signal is therefore $G(V_s, T_{high})(nT_s)$. The dependence with the temperature of the fast redistribution of carriers in the semiconductor is therefore removed from the feedback signal.
- 2nd objective: implement a PWM control allowing to compensate the slow variations in V_s due to changes in the adsorbed species.

The control keeps constant the conductivity of the sensing layer, measured at constant temperature (T_{high}), by adapting the average temperature generated by the PWM signal. This PWM signal, or the average temperature generated, is the new sensor output. The advantage of using the average temperature as system output is that it is a physical magnitude. Since the temperature transitions are shorter than 5 ms, the average temperature is calculated assuming constant temperature profiles during the time intervals corresponding to each T_{low} and T_{high} values (10 ms of transient responses over a time slot of 250 ms).

The main contribution in this work is to prove that the same type of active controls can use as feedback signal the reactance of the sensing layer, instead of the conductance. It has been shown in [21] that reactance measurements (dielectric excitation) can increase linearity and reduce recovery time.

3 SENSOR DESCRIPTION

The experiments done in this work are made with two different MOX sensors, to test the new control technology for different gases. The first one is the CCS801, currently fabricated by ScioSense [29], and uses a MEMS membrane to support and heat the sensing layer. This sensor can detect a wide range of volatile organic compounds (VOCs) such as ethanol or carbon monoxide. The second sensor is also based on a MEMS micro-hotplate. In this case, the micro-hotplates were implemented in double side polished p-type <100> Si substrates (300 µm in thickness). They were designed and fabricated at IMB-CNM-CSIC, following different microfabrication steps including implantation, photolithography, metallization, lift-off and rear side etching of the substrate to define the membranes [30]. Mounted MEMS were placed into an AACVD cold-wall reactor and the heating elements of the membranes were connected to a power supply, so membranes were kept a temperature of 400°C during the whole synthesis process. Tungsten hexacarbonyl ($W(CO)_6$) 97% purity and hydrogen tetrachloroaurate ($HAuCl_4 \cdot 3H2O$) 99.9% purity from Sigma-Aldrich were used for obtaining a film of randomly oriented tungsten oxide nanowires loaded with Au nanoparticles on the heated membranes in a single step. At first, 50 mg $W(CO)_6$ and 2.5 mg of $HAuCl_4 \cdot 3H2O$ are dissolved in an acetone:methanol (ratio 3:1) mixture. This solution is placed under ultra-sonication to form an aerosol, which is input to the reactor chamber using a 0.5 L/min nitrogen flow. More details on this vapour-solid growth can be found elsewhere [31-32]. Full details on the morphology and chemical composition of the Au-loaded WO_3 nanowire films can be found in [32].

4 EXPERIMENTAL RESULTS

The measurement setup described in **Fig. 5** has been used. The gas sensor is placed inside an airtight chamber. Mass flow controllers (MFC) keep a constant flow of maximum 300 mL/min inside the chamber. The gases used are: zero-grade dry air and ethanol (C_2H_5OH) balanced in dry air for the experiments conducted using the CCS801 sensors; and zero-grade dry air and ammonia balanced in dry air (NH_4) for measurements involving the Au nanoparticle loaded WO_3 sensor. The chamber has a dead volume of 4 mL and an exhaust hole to ensure the renovation of the gas flow.

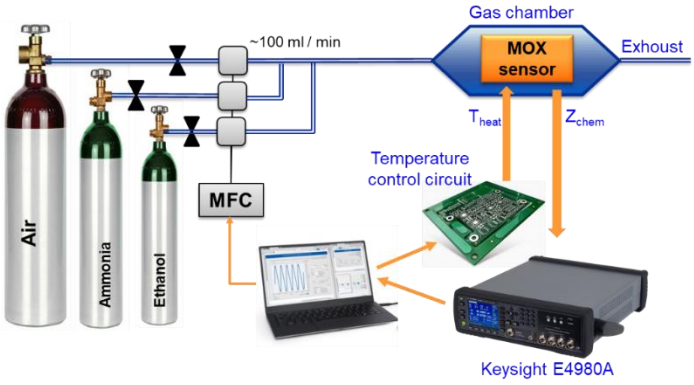

Fig. 5. Description of the experimental setup.

The sensing layer impedance of the sensor is acquired with an impedance analyzer Keysight E4980A. This instrument sends the information to the PC and the data is processed in real-time. The program takes a control decision and sends it to a STM32F303RE microcontroller, which generates the required temperature waveform signals to the temperature control circuit in **Fig. 1**.

4.1 First sensor: CCS801

To characterize the CCS801 sensor, a frequency sweep experiment was carried out for different gas concentrations of ethanol (see **Fig.6)**. As it can be seen, the sensor is sensitive to changes in gas concentration both in the real part (resistance) and imaginary part (reactance) of the sensor.

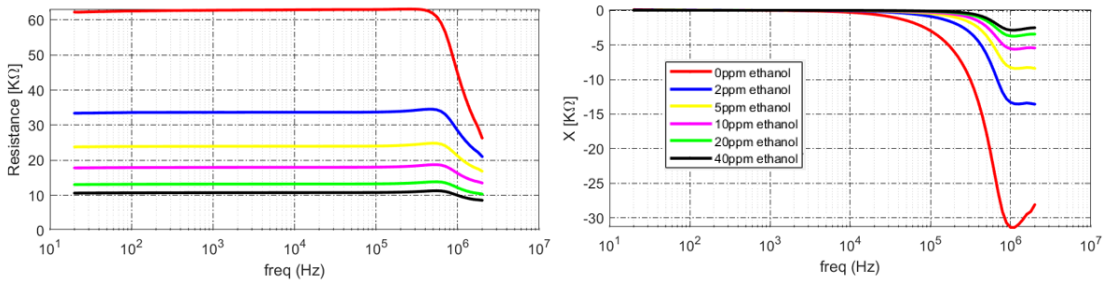

Fig. 6. CCS801 frequency sweep for different ethanol concentrations. Resistance (left) and reactance response (right).

An experiment was performed to compare the sensor response under closed-loop and open-loop configurations, in both cases using the reactance of the sensor measured at 30kHz. **Fig.7 (left)** shows the open-loop reactance response at constant temperature of 200°C, to 0.25 ppm and 0.5 ppm of ethanol. Between both concentrations, the system was exposed to dry air to observe baseline recovery time. The same experiment is replicated in **Fig.7 (right)**, but this time applying the reactance-based closed-loop control described in the previous section (T_{High}=200°C and T_{Low}=150°C). The output of **Fig.7 (right)** is the mean temperature applied to the sensing layer during the first 100 ms of the temperature waveform (when temperature changes are made).

In both experiments, the measurement frequency, 30 kHz, was chosen in order to have a good stability of the control. Frequencies near 100 kHz could generate saturation events when exposed to changes in gas concentration, and in the low frequency range, the control output was noisy since the system is not very sensitive to different gas concentrations. A guideline on how to set up the control parameters in these types of controls can be found in [28]. One important parameter is the target value of the control, which is typically set to avoid saturation events and also taking into account whether the atmosphere will present reducing or oxidizing gases (the control increases the output average temperature if an n-type semiconductor is exposed to reducing agents, while the opposite behavior is shown in case of oxidizing gases), [33].

Two improvements can be seen by comparing the results of the two figures. The first one is related to the removal of the drift. While there is an ascendant trend in the open-loop measurement throughout the experiments, this effect is mitigated by using the closed-loop control. The other improvement is the baseline recovery time, which is one of the main issues of the resistance controls seen in other works. The recovery time when the closed-loop control is used is reduced to 5 minutes, which compares favorably to a recovery time that well exceeds 10 minutes for the sensor operated under open-loop conditions. The complete recovery of the baseline under closed-loop conditions explains why the drift is removed. The rise and fall time constants in open-loop configuration are 41.11 s and 213.97 s respectively, while working in closed loop are 41.4 s and 34.1 s (one exponential model in all cases).

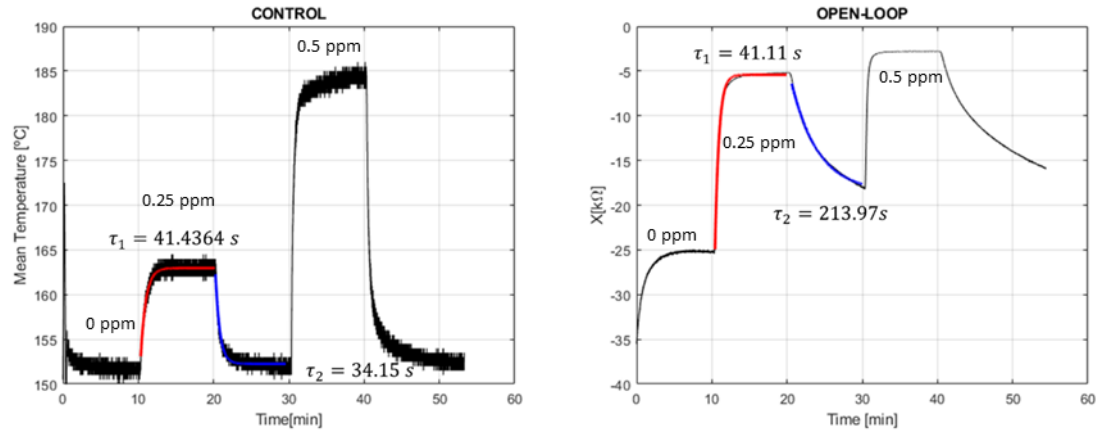

Fig. 7. Comparison between open-loop (right) and closed-loop (left) measurements for CCS801 sensor at f=30 kHz. Experiment made with ethanol balanced in dry air. The time constants associated with the rise and fall times have been added to the graph (obtained by fitting from the red and blue parts of the curves).

The behaviour of the sensors working under closed-loop control is generally complex. It can be seen in **Fig. 7** that the linearity of the sensor has improved, compared with open-loop reactance-based measurements. On the other hand, the selection of the operating temperatures T_{low} and T_{high}, determines the limits on the gas concentrations changes not triggering saturation events. Open loop characterization may be used for adequate parameter selection in these controls [28]. On the other hand, the requirements for sensor electronics are generally more demanding. For example, even though sigma-delta modulation generates a zero in the quantization noise at zero frequency, it can be seen in **Fig. 7 (right)** that the signal is noisier. In this case, this effect has been caused by the need of a long measuring time for the reactance of the layer (larger 'chattering' amplitude) and it is not intrinsic to the controls. As an example, it has been possible to obtain closed-loop responses with very little noise, as shown in [28]. Additionally, there are 100 quantization levels produced by the PWM signal, at an output rate of 4Hz. Since the real bandwidth of the sensor is well below this sampling frequency, by simply averaging 10 consecutive samples, for example, it is possible to obtain 1000 quantization levels, at a 0.25Hz rate. This approach has been adopted in the measurements shown in this work, and it is typically used in oversampled converters such as sigma-delta modulators.

Finally, another experiment with a higher flow, 300mL/min, has been made. The result can be seen in Fig. 8, in which the open-loop and closed-loop responses of the sensor can be seen under these new conditions. This experiment consists of 1-hour steps applying zero-grade dry air and 1-hour applying different concentrations of ethanol balanced in dry air. In this case, the temperatures used have been T_{High}=340°C and T_{Low}=240°C. As it can be seen the time response of the sensor has been improved. The baseline recovery time has been drastically reduced when the control is applied. Using a larger flow (300mL/min), therefore, did not have any significant impact on the results.

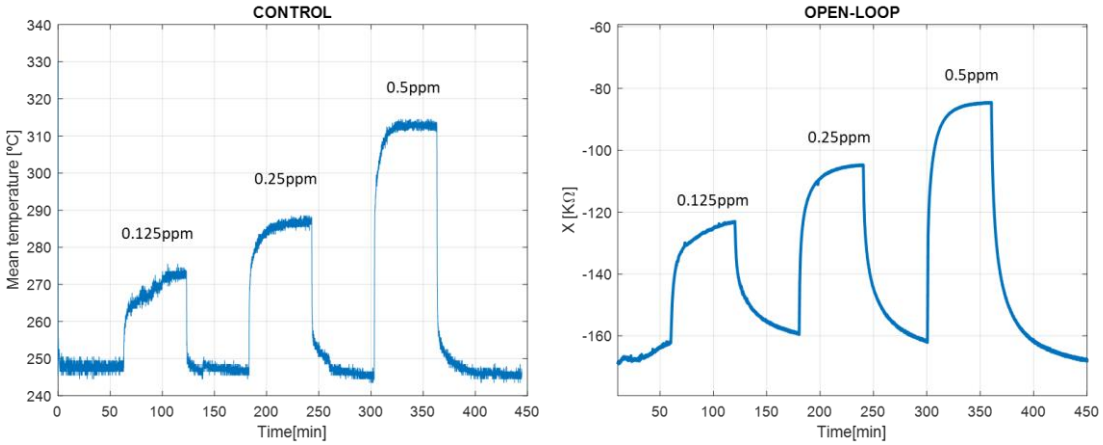

Fig. 8. Comparison between open-loop (left) and closed-loop (right) measurements for CCS801 sensor at f=30 kHz with 300mL/min of gas flow. Experiment made with different ethanol balanced in dry air concentrations.

4.2 Second sensor: in-house Au-WO_3 sensor

In this section, the sensing layer is made of WO_3 nanowires loaded with Au nanoparticles. This sensor has been designed to be sensitive to NH_3. A first experiment was performed with the sensor working at a constant temperature T_{High}=300ºC in an open-loop configuration (**Fig. 9**). As it had been done with the CCS801 sensor, a frequency sweep experiment was carried out to see the sensing layer impedance variations due to changes in ammonia concentration. As in all the other experiments done, the flow was kept constant at 100 mL/min. The results obtained show that the sensor is sensitive to ammonia concentration changes. Both real part of the sensor impedance (resistance) and imaginary part (reactance) change when the sensor is exposed to different concentrations of ammonia. The range of frequencies where the sensor is more sensitive is between 10 kHz and 100 kHz.

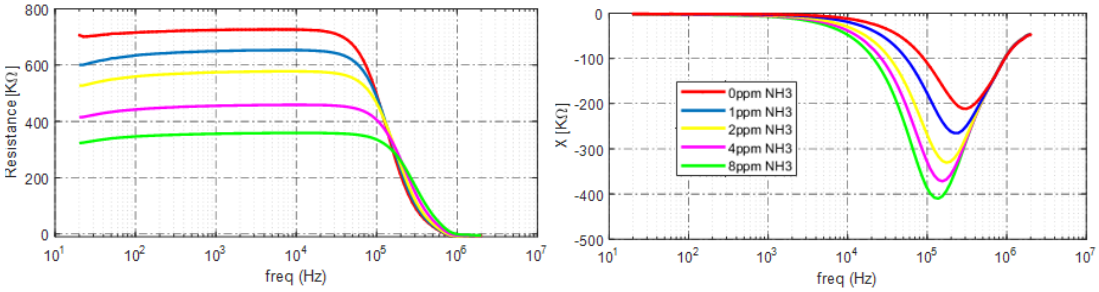

Fig. 9. URV sensor frequency sweep for different NH_3 concentrations. Resistance (left) and reactance response (right).

Fig. 10 shows the behavior over time of the sensor. Two cycles consisting of 1-hour exposure to 1 ppm of ammonia followed by 1-hour recovery in pure dry air were applied. At the beginning of the experiment, the sensor was stabilized for 1-hour under dry air. In all experiments, a frequency of 30 kHz and a voltage of 4V AC were applied. **Fig.10 (left)** shows the performance of the open-loop operation and **Fig.10 (right)** shows the closed-loop control response. In this case, the temperatures chosen are T_{High}=300ºc and T_{Low}=200ºC. Comparing the results, it can be seen that the drift and recovery times are improved by applying the proposed control.

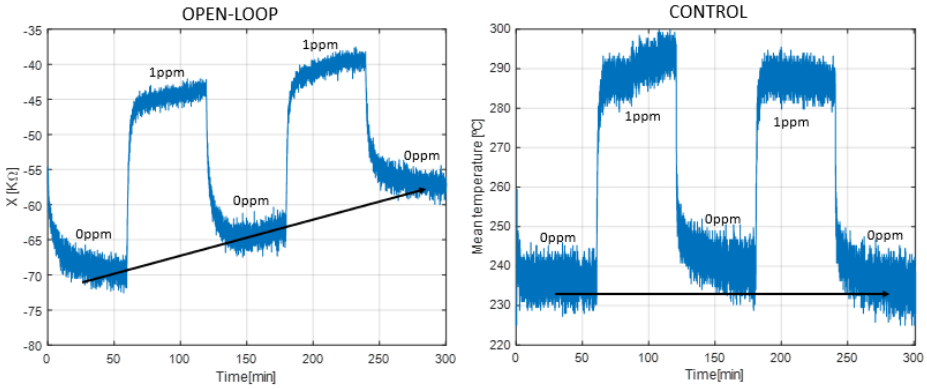

Fig. 10. Comparison between open-loop (left) and closed-loop (right) measurements for URV sensor at f=30kHz. Experiment made with ammonia balanced in dry air. The black line placed on the two graphs shows the drift correction.

Another improvement can be observed, as illustrated in **Fig. 11**. The time needed to reach the steady-state plateau of ammonia response is reduced. While the time needed under closed-loop control is about 5 minutes, for the open-loop operation, the sensor has not yet reached the steady-state after 10 minutes. This result is comparable to the one achieved for the commercial sensor and indicates that the closed-loop control improves response and recovery dynamics and thus, improves response stability. The rise time constants in open-loop and closed-loop configurations are 95.15 s and 46.05 s, respectively (one exponential model).

The measurements in Fig. 10 reflect the fact the MOX gas sensors generally present complex and long-term memory effects (such as drifts). Fig. 10 (left) may be showing a mixture of drift and exponential responses. In any case, MOX gas sensors generally present complex and long-term memory effects (such as drifts). An example of complex behavior, for example, can be found in Fig. 10 (right), where the sensor response to the first gas concentration pulse is slightly different to the second one. Additionally, another effect is that depending on the internal mechanisms driving conductance changes in the sensing layer, the response time reduction may differ from one sensor to another. For example, the response time reduction has been more noticeable in the case of the first sensor. This effect has been observed in thermal sensors: two 3D thermal anemometers presenting similar open-loop responses may present radically different response times while working under closed loop [24]. By analyzing the internal thermal signatures and applying sliding mode control theory, it has been possible to explain and model the different behavior.

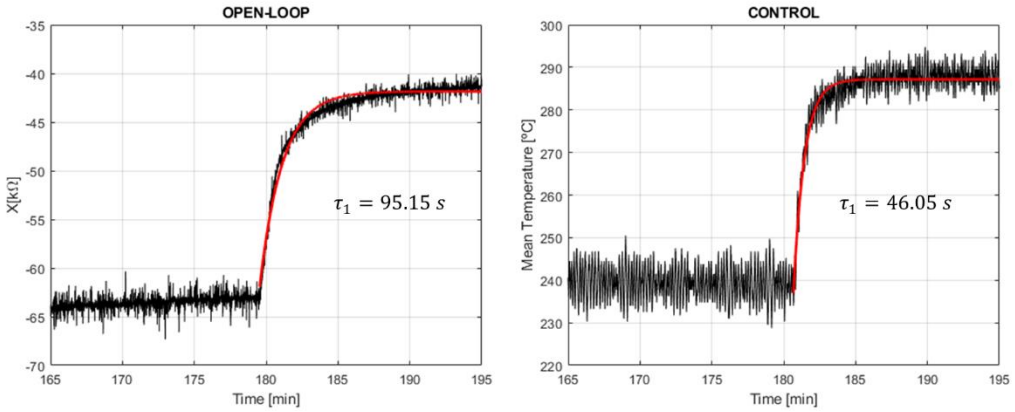

Fig. 11. Zoom on the second rise transition of fig.8. Comparison between open-loop (left) and closed-loop (right) measurements for URV sensor at f=30kHz. The rising time constants (for a one exponential model) have been added to the plot.

Discussion: The use of the reactance of the sensor as proposed in [25] has been shown to improve linearity and reduction of the recovery times, as compared with the typical conductance measurements. In this work we have applied for the first time closed loop control techniques using the reactance of the layer, measured at constant temperature, as feedback signal. The main advantage observed is the reduction of the response time and the recovery time. In this and the previous works it has generally been observed that the time response is always reduced, as compared with operating the sensor in open-loop configuration.

5 CONCLUSIONS

The results of applying temperature control to the imaginary part of the sensing layer impedance have been shown. This technique has been applied to both a commercial MEMS MOX sensor (the CCS801) and to an in-house developed MOX MEMS sensors (the sensitive film consists of $W0_3$ nanoneedles functionalized with Au nanoparticles). This results in a clear improvement in sensor dynamics as response and recovery times are shortened by a factor higher than 2 (in case of the commercial sensor, recovery time is reduced by a factor of 6). Improved dynamics help to virtually eliminate response drift. To the best knowledge of the authors, this is the first time that a control based on dielectric excitation is applied to MOX gas sensors.

FUNDING

Funded in part by MININN, grants no. RTI2018-098728-B-C33, RTI2018-101580-B-I00 and PID2019-107697RB-C42. E.L supported by ICREA Academia Award, 2018 Edition.

REFERENCES

[1] Mirzaei, Ali, S. G. Leonardi, and Giovanni Neri, "Detection of hazardous volatile organic compounds (VOCs) by metal oxide nanostructures-based gas sensors: A review." *Ceramics international* 42.14 (2016): 15119-15141.

[2] T.D. Durbin, R.D. Wilson, J.M. Norbeck, J.W. Miller, T. Huai, S.H. Rhee, Estimates of the emission rates of ammonia from light-duty vehicles using standard chassis dynamometer test cycles, Atmos. Environ. 36 (2002) 1475–1482.

[3] R. Moos, R. Muller, C. Plog, A. Knezevic, H. Leye, E. Irion, T. ¨ Braun, K.-J. Marquardt, K. Binder, Selective ammonia exhaust gas sensor for automotive applications, Sens. Actuators B 83 (2002) 181–189.

[4] Mount, George H., et al. "Measurement of atmospheric ammonia at a dairy using differential optical absorption spectroscopy in the mid-ultraviolet." *Atmospheric Environment* 36.11 (2002): 1799-1810.

[5] Roney, Nickolette, et al. "Toxicological profile for ammonia." Report by the US Dept. of Health and Human Services, (2004), https://www.atsdr.cdc.gov/toxprofiles/tp126.pdf

[6] Timmer, Björn, Wouter Olthuis, and Albert Van Den Berg. "Ammonia sensors and their applications—a review." *Sensors and Actuators B: Chemical* 107.2 (2005): 666-677.

[7] Nazemi, Haleh, et al. "Advanced micro-and nano-gas sensor technology: A review." *Sensors* 19.6 (2019): 1285.

[8] Vergara, Alexander, et al. "Multifrequency interrogation of nanostructured gas sensor arrays: A tool for analyzing response kinetics." *Analytical chemistry* 84.17 (2012): 7502-7510.

[9] E. Llobet, J. Brezmes, X. Vilanova, J.E. Sueiras, X. Correig, Qualitative and quantitative analysis of volatile organic compounds using transient and steady-state responses of a thick-film tin oxide gas sensor array, Sens. Actuators B Chem. 41 (1997) 13–21.

[10] C. Di Natale, S. Marco, F. Davide, A. D'Amico, Sensor-array calibration time reduction by dynamic modelling, Sens. Actuators B Chem. 25 (1995) 578–583

[11] A. Pardo, S. Marco, J. Samitier, Nonlinear inverse dynamic models of gas sensing systems based on chemical sensor arrays for quantitative measurements, Instrum. Meas. IEEE Trans. 47 (1998) 644–651.

[12] Djedidi, O., Djeziri, M. A., Morati, N., Seguin, J.-L., Bendahan, M., Contaret, T. (2021). Accurate detection and discrimination of pollutant gases using a temperature modulated MOX sensor combined with feature extraction and support vector classification. Sens. Actuators, B, 339, 129817.

[13] R. Gosangi, R. Gutierrez-Osuna, Active temperature modulation of metal-oxide sensors for quantitative analysis of gas mixtures, Sens. Actuators B Chem. 185 (2013) 201–210.

[14] Ji, Hanyang, et al. "Qualitative and quantitative recognition method of drug-producing chemicals based on SnO2 gas sensor with dynamic measurement and PCA weak separation." Sens. Actuators, B, vol. 348, p. 130698, 2021.

[15] J. Fonollosa, S. Sheik, R. Huerta, S. Marco, Reservoir computing compensates slow response of chemosensor arrays exposed to fast varying gas concentrations in continuous monitoring, Sens. Actuators B Chem. 215 (2015) 618–629.

[16] S. De Vito, A. Castaldo, F. Loffredo, E. Massera, T. Polichetti, I. Nasti, P. Vacca, L. Quercia, G. Di Francia, Gas concentration estimation in ternary mixtures with room temperature operating sensor array using tapped delay architectures, Sens. Actuators, B Chem. 124 (2007) 309–316.

[17]Ahmadou, Diaa, et al. "Reduction of drift impact in gas sensor response to improve quantitative odor analysis." *2017 IEEE International Conference on Industrial Technology (ICIT)*. IEEE, 2017.

[18] T. Baur, C. Schultealbert, A. Schütze, T. Sauerwald, Novel method for the detection of short trace gas pulses with metal oxide semiconductor gas sensors, Journal of Sensors and Sensor Systems. 7 (2018) 411–419.

[19] C.-D. Kohl, T. Wagner, eds., Gas Sensing Fundamentals, Springer Berlin Heidelberg, Berlin, Heidelberg, 2014.

[20] T. Kammerer, M. Engel, A. Schutze, An intelligent fuel sensor based on a microstructured gas sensor, Proceedings of IEEE Sensors 2003, pp. 1064-1069.

[21] Dominguez-Pumar, M., Kowalski, L., Calavia, R., & Llobet, E. (2016). Smart control of chemical gas sensors for the reduction of their time response. *Sensors and Actuators B: Chemical*, *229*, 1-6.

[22] Kowalski, L., Pons-Nin, J., Navarrete, E., Llobet, E., & Domínguez-Pumar, M. (2018). Using a second order sigma-delta control to improve the performance of metal-oxide gas sensors. *Sensors*, *18*(2), 654.

[23] Kowalski, L., Navarrete, E., Llobet, E., & Dominguez-Pumar, M. (2019, June). Control of Surface Potential in WO 3 Gas Sensors Using UV Light. In *2019 20th International Conference on Solid-State Sensors, Actuators and Microsystems & Eurosensors XXXIII (TRANSDUCERS & EUROSENSORS XXXIII)* (pp. 1258-1261). IEEE.

[24] M.-T. Atienza, L. Kowalski, S. Gorreta, V. Jiménez, L.M. Castañer, M. Domínguez-Pumar, Sliding mode analysis applied to improve the dynamical response of a spherical 3D wind sensor for Mars atmosphere, Sensors and Actuators A: Physical. 267 (2017) 342–350.

[25] Potyrailo, R. A., Go, S., Sexton, D., Li, X., Alkadi, N., Kolmakov, A., ... & McConnell, P. (2020). Extraordinary performance of semiconducting metal oxide gas sensors using dielectric excitation. *Nature Electronics*, *3*(5), 280-289.

[26] J.H. Watmuff, An investigation of the constant-temperature hot-wire anemometer, *Exp. Th. and Fluid Science* 11, (1995): 117-134.

[27] P. Ligęza, Constant-bandwidth constant-temperature hot-wire anemometer, Review of Scientific Instruments. 78 (2007) 075104.

[28] Dominguez-Pumar, M., Olm, J. M., Kowalski, L., & Jimenez, V. (2020). Open loop testing for optimizing the closed loop operation of chemical systems. Comput. Chem. Eng., 135, 106737.

[29] CCS801 Ultra-Low Power Analog VOC Sensor for Indoor Air Quality Monitoring CCS801 Datasheet: https://www.sciosense.com/wp-content/uploads/documents/SC-001255-DS-2-CCS801B-Datasheet-Revision-2.pdf

[30] Stoycheva, T.; Annanouch, F.; Gràcia, I.; Llobet, E.; Blackman, C.; Correig, X.; Vallejos, S. Micromachined Gas Sensors Based on Tungsten Oxide Nanoneedles Directly Integrated via Aerosol Assisted CVD. Sens. Actuators, B 2014, 198, 210–218.

[31] Vallejos, S., Umek, P., Stoycheva, T., Annanouch, F., Llobet, E., Correig, X. de Marco, P., Bittencourt, C. and Blackman, C. (2013). Single-Step Deposition of Au- and Pt-Nanoparticle-Functionalized Tungsten Oxide Nanoneedles Synthesized Via Aerosol-Assisted CVD, and Used for Fabrication of Selective Gas Microsensor Arrays. Advanced Functional Materials, 23(10), 1313–1322.

[32] Navarrete È, Bittencourt C, Noirfalise X, Umek P, González E, Güell F, Llobet E. Title: WO3 nanowires loaded with cobalt oxide nanoparticles, deposited by a two-step AACVD for gas sensing applications. Sensors and Actuators,B: Chemical 298, 126868. (2019

[33] Monge-Villora, O., Dominguez-Pumar, M. and Olm, J.M. (2018). Analysis of the dynamics of an active control of the surface potential in metal oxide gas sensors. Computers & Chemical Engineering, [online] 113, pp.1–10.